ISSN 1392–1320 MATERIALS SCIENCE (MEDŽIAGOTYRA). Vol. 24, No. 4. 2018

A Novel Porous $Sm_2Ti_2O_7$ Material Synthesized in Sol-gel Process Using Polyethylene Glycol 4000 as Template

Wenjie ZHANG *, Haolun LI, Ling DU

School of Environmental and Chemical Engineering, Shenyang Ligong University, Shenyang 110159, China

crossref http://dx.doi.org/10.5755/j01.ms.24.4.18213

Received 21 May 2017; accepted 16 November 2017

A sol-gel method was used to synthesise $Sm_2Ti_2O_7$ photocatalysts. It was found that crystalline formation of pyrochlore phase $Sm_2Ti_2O_7$ is promoted by addition of the PEG4000 template. Reduced particles aggregation was observed in the porous $Sm_2Ti_2O_7$. The addition of PEG4000 led to a slight increase in bandgap energy of $Sm_2Ti_2O_7$. The conduction band edge and valence band edge positions of porous $Sm_2Ti_2O_7$ were – 0.37 V and 2.75 V, respectively. The first order kinetic reaction constant is 0.01637 min^{-1} on the porous $Sm_2Ti_2O_7$, while the reaction constant was 0.00431 min^{-1} on the bare $Sm_2Ti_2O_7$.

Keywords: photocatalysis, $Sm_2Ti_2O_7$, sol-gel, PEG4000, porous.

1. INTRODUCTION

Photocatalytic technology is an advanced oxidation method in removal of environmental pollutants [1 – 3]. The preparation of novel photocatalytic materials with promising activity is the key focus with the purpose of achieving satisfactory results in industrial wastewater treatment. The titanate materials, such as $CaTiO_3$ [4], $SrTiO_3$ [5], $Gd_2Ti_2O_7$ [6, 7], $Bi_4Ti_3O_{12}$ [8], $La_2Ti_2O_7$ [9], $Ce_2Ti_2O_7$ [10], and $Sm_2Ti_2O_7$ [11, 12] have been studied as potential photocatalysts.

$Sm_2Ti_2O_7$ is used as an electronic material [13, 14]. However, the material was usually prepared by solid state reaction, so that high temperature thermal treatment is always unavoidable in preparation of $Sm_2Ti_2O_7$. $Sm_2Ti_2O_7$ is usually lack of porous structure and is not considered to be a promising photocatalyst due to poor adsorption capacity and weak quantum efficiency. Porous structure is hard to be introduced into $Sm_2Ti_2O_7$ prepared by solid state reaction.

A long-chain macromolecular compound, polyethylene glycol (PEG), is a widely used template agent in modifying the structure of materials [15]. Besides abundant pores formed in the synthesized materials after thermal treatment, the use of PEG can put extra effect on crystal formation as well [16]. We reported the enhanced photocatalytic activity of $Ce_2Ti_2O_7$ modified with PEG4000 by sol-gel method [10].

In this work, we report the preparation and properties of $Sm_2Ti_2O_7$ using PEG4000 as template in a sol-gel process. Photocatalytic degradation of a commercial dye, Reactive Brilliant Red X3B (RBR-X3B), was measured to evaluate the effects of PEG4000 on photocatalytic activity of $Sm_2Ti_2O_7$. The PEG4000 modified $Sm_2Ti_2O_7$ were characterized by XRD, SEM and UV-Vis diffuse reflectance methods. The aim of this work is to clarify the effects of PEG4000 on physic-chemical properties of the $Sm_2Ti_2O_7$ and promote the activity of this material.

2. MATERIALS AND METHODS

2.1. Synthesis of PEG4000 modified $Sm_2Ti_2O_7$

$Sm_2Ti_2O_7$ was prepared by a sol-gel method as similar as our previous work [17]. All the starting materials are analytical reagents. 1.5 g PEG4000 and 1.1112 g samarium nitrate were dissolved in 8 mL ultrapure water, followed by the addition of 8 mL acetic acid. 0.85 mL tetrabutyl titanate and 8 mL ethanol were mixed together to form another solution. After the two solutions were mixed together, 2 mL glycol was added to make a transparent sol. The n(La)/n(Ti) ratio was 1:1 in the final sol. The sol was stirred at 70 °C to form a yellow gel. The gel was dried in a 110 °C furnace for 24 h and then was ground into fine powders. The powders were put into an oven in which temperature increased from room temperature to 900 °C at a rate of 5 °C/min. After 3 h of calcination, the powders were ground again before measuring.

2.2. Characterization methods

Crystal structure of the materials was analyzed by D8 Advance X-ray diffractometer at 40 kV and 40 mA for monochromatized Cu Kα (λ = 1.5416 Å) radiation [10]. The software GSAS was used for the Rietveld Refinement. The surface morphology was observed by QUANTA 250 scanning electron microscope at an accelerating voltage of 30 kV. A thin layer of gold was coated on the samples to avoid charging. UV-Vis diffuse reflectance spectra were recorded by LAMBDA 35 UV-Vis spectrometer equipped with an integrating sphere. The scan rate was 480 nm/min. The spectra were measured using $BaSO_4$ as a reference and were transformed from reflection to absorbance by the Kubelka-Munk method [18].

* Corresponding author. Tel.: +86-13609880790.
E-mail address: *wjzhang@aliyun.com* (W. Zhang)

2.3. Photocatalytic degradation of RBR-X3B

Photocatalytic degradation of RBR-X3B on the $Sm_2Ti_2O_7$ samples was performed in a lab scale reactor [19]. The chemical formula of RBR X-3B is $C_{19}H_{10}Cl_2N_6Na_2O_7S_3$. 50 mL RBR-X3B solution and 20 mg $Sm_2Ti_2O_7$ were put into a 100 mL quartz beaker and stirred for 30 min in the dark to ensure adsorption-desorption equilibrium. The initial concentration of RBR-X3B aqueous solution was 30 mg/L. The light source was a 20 W UV-light lamp irradiating at $\lambda = 253.7$ nm with the irradiation intensity of 1200 $\mu W/cm^2$. A 721E spectrophotometer was used to measure the absorbance of the RBR-X3B solution. The UV lamp was turned on to trigger photocatalytic degradation of RBR-X3B after adsorption-desorption equilibrium.

3. RESULTS AND DISCUSSION

prepared using different amount of PEG4000. Although the addition amount of the template is different in the precursor, the diffraction patterns of all the samples are in accordance to the pattern of JCPDS No.73-1699. The pyrochlore phase $Sm_2Ti_2O_7$ is in the Fd3m lattice of cubic crystal system. The addition of PEG4000 does not result in phase transformation of pyrochlore phase $Sm_2Ti_2O_7$, nor does it introduce any other impurities into the materials. Meanwhile, as can be seen from the patterns, the diffraction intensities become stronger after introducing PEG4000. Crystalline formation of pyrochlore phase $Sm_2Ti_2O_7$ can be promoted by the addition of the template. The adhesion of PEG4000 molecules on the surface of $Sm_2Ti_2O_7$ crystal nuclei may provide new nucleation center and lower down the required energy for further nucleation [15, 16].

Scherrer formula is used to calculated crystallite size of $Sm_2Ti_2O_7$ in the samples, based on the data of the preferred (222) plane. The bare $Sm_2Ti_2O_7$ without PEG4000 has a crystallite size of 35.4 nm, while the crystallite size is 37.0 nm for the porous $Sm_2Ti_2O_7$ using 1.5 g PEG4000. A slight enlargement in crystallite size of $Sm_2Ti_2O_7$ occurs after using PEG4000. This is due to prohibited crystal growth after using template in sol-gel precursor. The key purpose of using template in sol-gel synthesizing process is to introduce porous structure in the $Sm_2Ti_2O_7$ material. Meanwhile, the PEG4000 template can also put effects on $Sm_2Ti_2O_7$ crystal growth of the material.

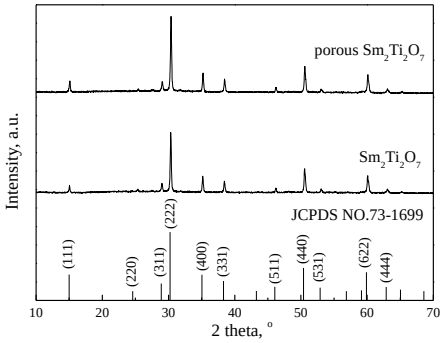

Fig. 1. XRD patterns of $Sm_2Ti_2O_7$ samples

Surface morphology of the $Sm_2Ti_2O_7$ materials is influenced by the addition of PEG4000 template, as presented in Fig. 2. The bare $Sm_2Ti_2O_7$ without PEG4000 is composed of irregular particles in the size as large as 5 μm. Particle refinement is caused by the addition of PEG4000. Tetrabutyl titanate molecules are adsorbed on the macromolecular PEG4000 before hydrolysis in the precursor. Steric hindrance effect acts to prohibit hydrolysis of tetrabutyl titanate molecules and particles aggregation as well.

Titanate is usually synthesized during high temperature thermal treatment. The samples are calcinated at 900 °C in this work. Such high calcination temperature is favored by crystal growth and particles aggregation. However, large particles have low efficiency in absorbing incoming irradiating photons and therefore is not a suitable form during photocatalytic reaction. The use of template is capable of introducing porous structure in the material. However, it does not mean that more template is better for promoting the activity.

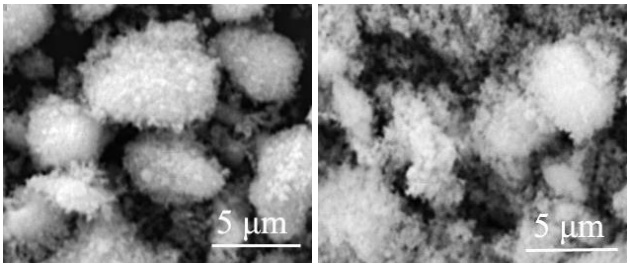

a b

Fig. 2. SEM images of $Sm_2Ti_2O_7$ and porous $Sm_2Ti_2O_7$ using 1.5 g PEG 4000

UV-Vis diffuse reflectance spectra of $Sm_2Ti_2O_7$ are given in Fig. 3 to show the effect of PEG4000 addition on band edge structure of the materials. Kubelka-Munk theory is used to calculate bandgap in the $Sm_2Ti_2O_7$ samples [18]. The band edge of porous $Sm_2Ti_2O_7$ shifts to shorter wavelength after the addition of PEG4000, due to the refinement of $Sm_2Ti_2O_7$ particles. The bare $Sm_2Ti_2O_7$ sample without PEG4000 has a bandgap of 2.86 eV, as calculated through the formula

$$(\alpha h\nu) = A(h\nu - Eg)^n, \quad (1)$$

where α, h, ν, A and Eg are the absorption coefficient, Planck constant, light frequency, proportionality constant and bandgap energy, respectively [20]. The bandgap of the porous $Sm_2Ti_2O_7$ is 3.12 eV.

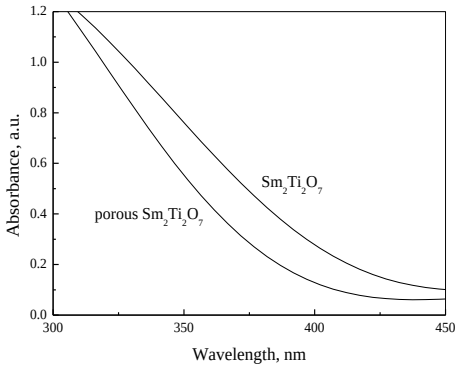

Fig. 3. UV-Vis diffuse reflectance spectra of $Sm_2Ti_2O_7$ and porous $Sm_2Ti_2O_7$

The addition of PEG4000 in the sol-gel precursor leads to a slight increase in bandgap energy of $Sm_2Ti_2O_7$. Normally, the enlarged bandgap is not beneficial to absorption of light at long wavelength. However, since the main irradiating wavelength of the UV lamp used in this work is 253.7 nm, the incoming photons have enough energy to initiate all the $Sm_2Ti_2O_7$ samples despite the difference in bandgap energy. On the other hand, the PEG4000 modified $Sm_2Ti_2O_7$ sample cannot be as effective as the bare sample in absorbing photons in visible light region.

The conduction band edge and valence band edge of photocatalyst can be predicted according to equations [21,22]:

$$E_{CB} = X - E^C - Eg/2; \quad (2)$$

$$E_{VB} = E_{CB} + Eg, \quad (3)$$

where E_{CB} and E_{VB} are the positions of conduction and valence band edges, respectively. X is the absolute electronegativity of semiconductor. E^C is the energy of the free electrons on the hydrogen scale about 4.5 eV, and Eg is the band gap energy. The predicted band edge positions and photocatalytic mechanism of porous $Sm_2Ti_2O_7$ using 1.5 g of PEG4000 are shown in Fig. 4. The calculated conduction band edge position of porous $Sm_2Ti_2O_7$ is – 0.37 V, in addition to the valence band edge at 2.75 V. The oxidation potential of H_2O which can be oxidized to •OH radicals is 2.72 V [23]. Obviously, the conduction band potential is higher than the oxidation potential of H_2O, so that porous $Sm_2Ti_2O_7$ can directly utilize H_2O to produce hydroxyl radicals. OH^- can be oxidized to •OH radicals owing to its lower oxidation potential of 1.89 V. The porous $Sm_2Ti_2O_7$ can produce more •OH radicals and display strong photocatalytic degradation activity. The valence band potential of porous $Sm_2Ti_2O_7$ is – 0.37 V, which is lower than the reduction potential of O_2 (– 0.13 V). O_2 can be reduced to O_2^-• [24].

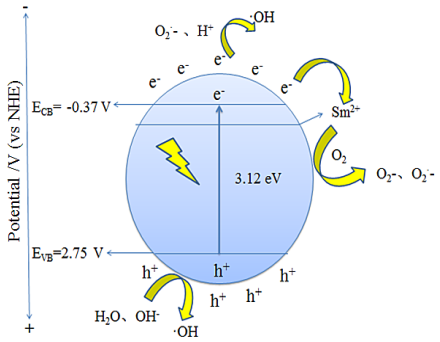

Fig. 4. Schematic illustration of the photocatalytic mechanism of porous $Sm_2Ti_2O_7$ on degradation of RBR X-3B

It is supposed that Sm^{2+} can act as low potential trap for photogenerated electrons. The trapped electrons might react with the adsorbed O_2 to form O^{2-} and even the strongly oxidative $\cdot O^{2-}$ species. Meanwhile, O^{2-} can also react with surface hydroxyl to form hydroxyl radical·OH. The occurrence of low potential trap will eventually increase the amount of reactive oxygen species, and therefore inhibits the recombination of photogenerated electrons and holes. As a result, quantum efficiency is promoted.

Fig. 5 compares photocatalytic degradation of RBR-X3B on the bare $Sm_2Ti_2O_7$ and porous $Sm_2Ti_2O_7$ samples. Enhanced activity on RBR-X3B degradation is found in the figure after using PEG4000. As much as 84.3 % of the initial dye molecules can be degraded on the porous $Sm_2Ti_2O_7$ after 120 min of irradiation, while the degradation efficiency is only 34.2 % on the bare $Sm_2Ti_2O_7$. The first order kinetic reaction constant is 0.01637 min^{-1} on $Sm_2Ti_2O_7$ with 1.5 g PEG4000, as compared to 0.00431 min^{-1} on the bare $Sm_2Ti_2O_7$.

The mechanism in promoting the activity of $Sm_2Ti_2O_7$ after using PEG4000 template in sol-gel preparation may be complex. The sol-gel process occurs after tetrabutyl titanate is binded on PEG4000 molecule. The three-dimentional condensation polymerization is therefore separated by PEG4000 molecule. Reduced crystallization and particles aggregation are believed to be one of the major reasons. The refined $Sm_2Ti_2O_7$ powders can suspend well in RBR-X3B solution, which is beneficial to the absorption of the incoming irradiating photons. Nano-sized material usually has strong activity and becomes the research focus in many fields, although the bandgap energy of $Sm_2Ti_2O_7$ is enlarged after using PEG4000 template in this work.

The bare $Sm_2Ti_2O_7$ sample has a BET surface area as small as 3.9 m^2/g. The addition of PEG4000 can obviously improve the porous structure formation. BET surface area of the porous $Sm_2Ti_2O_7$ sample is 20.2 m^2/g. Enlarged surface area is beneficial to the absorption of incoming irradiation and therefore to improve the decoloration efficiency [8, 10].

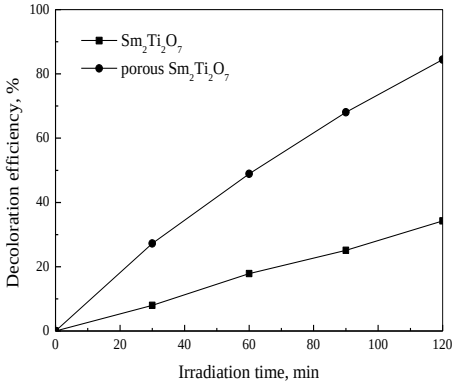

Fig. 5. Photocatalytic degradation of RBR-X3B on $Sm_2Ti_2O_7$ and porous $Sm_2Ti_2O_7$

4. CONCLUSIONS

The porous $Sm_2Ti_2O_7$ was synthesized in a sol-gel process after addition of PEG4000 template. The pyrochlore phase $Sm_2Ti_2O_7$ in the Fd3m lattice of cubic crystal system is not affected after using PEG4000. Particles aggregation is prohibited by the template. The addition of PEG4000 in the sol-gel precursor leads to a slight increase in bandgap energy of $Sm_2Ti_2O_7$. The porous $Sm_2Ti_2O_7$ PEG4000 has much improved photocatalytic activity and decoloration efficiency on RBR-X3B removal.

Acknowledgments

This work was supported by the Natural Science Foundation of Liaoning Province (No. 2015020186).

REFERENCES

1. **Fujishima, A., Rao, T., Tryk, D.** Titanium Dioxide Photocatalysis *Journal of Photochemistry and Photobiology C* 1 2000: pp. 1 – 21. https://doi.org/10.1016/S1389-5567(00)00002-2
2. **Zhang, W., Liu, Y., Pei, X., Chen, X.** Effects of Indium Doping on Properties of xIn-0.1%Gd-TiO_2 Photocatalyst Synthesized by Sol-gel Method *Journal of Physics and Chemistry of Solids* 104 2017: pp. 45 – 51. https://doi.org/10.1016/j.jpcs.2016.12.031
3. **Li, X., Fang, S., Ge, L., Han, C., Qiu, P., Liu, W.** Synthesis of Flower-like Ag/AgCl-Bi_2MoO_6 Plasmonic Photocatalysts with Enhanced Visible-light Photocatalytic Performance *Applied Catalysis B* 176 – 177 2015: pp. 62 – 69. https://doi.org/10.1016/j.apcatb.2015.03.042
4. **Lozano-Sánchez, L., Obregón, S., Díaz-Torres, L., Lee, S., Rodríguez-González, V.** Visible and Near-infrared Light-driven Photocatalytic Activity of Erbium-doped $CaTiO_3$ system *Journal of Molecular Catalysis A* 410 2015: pp. 19 – 25. https://doi.org/10.1016/j.molcata.2015.09.005
5. **Li, F., Yu, K., Lou, L., Su, Z., Liu, S.** Theoretical and Experimental Study of La/Ni co-doped $SrTiO_3$ Photocatalyst *Materials Science and Engineering: B* 172 (2) 2010: pp. 136 – 141. https://doi.org/10.1016/j.mseb.2010.04.036
6. **Zhang, W., Liu, Y., Li, C.** Photocatalytic Degradation of Ofloxacin on $Gd_2Ti_2O_7$ Supported on Quartz Spheres *Journal of Physics and Chemistry of Solids* 118 2018: pp. 144 – 149. https://doi.org/10.1016/j.jpcs.2018.03.019
7. **Zhang, W., Tao, Y., Li, C.** Sol-gel Synthesis of $Gd_2Ti_2O_7$/HZSM-5 Composite Photocatalyst for Ofloxacin Degradation *Journal of Photochemistry and Photobiology A: Chemistry* 364 2018: pp. 787 – 793. https://doi.org/10.1016/j.jphotochem.2018.07.022
8. **Chen, Z., Jiang, H., Jin, W., Shi, C.** Enhanced Photocatalytic Performance over $Bi_4Ti_3O_{12}$ Nanosheets with Controllable Size and Exposed {0 0 1} Facets for Rhodamine B degradation *Applied Catalysis B* 180 2016: pp. 698 – 706. https://doi.org/10.1016/j.apcatb.2015.07.022
9. **Chen, J., Liu, S., Zhang, L., Chen, N.** New $SnS_2/La_2Ti_2O_7$ Heterojunction Photocatalyst with Enhanced Visible-light Activity *Materials Letters* 150 2015: pp. 44 – 47. https://doi.org/10.1016/j.matlet.2015.02.134
10. **Zhang, W., Tao, Y., Li, C.** Effects of PEG4000 Template on Sol-gel Synthesis of Porous Cerium Titanate Photocatalyst *Solid State Sciences* 78 2018: PP. 16 – 21. https://doi.org/10.1016/j.solidstatesciences.2018.02.007
11. **Nashim, A., Parida, K.** Novel $Sm_2Ti_2O_7/SmCrO_3$ Heterojunction Based Composite Photocatalyst for Degradation of Rhodamine 6G Dye *Chemical Engineering Journal* 215 – 216 2013: pp. 608 – 615. https://doi.org/10.1016/j.cej.2012.11.025
12. **Uno, M., Kosuga, A., Okui, M., Horisaka, K., Yamanaka, S.** Photoelectrochemical Study of Lanthanide Titanium Oxides, $Ln_2Ti_2O_7$ (Ln = La, Sm, and Gd) *Journal of Alloys and Compounds* 400 2005: pp. 270 – 275. https://doi.org/10.1016/j.jallcom.2005.04.004
13. **Jafar, M., Sengupta, P., Achary, S., Tyagi, A.** Phase Evolution and Microstructural Studies in $CaZrTi_2O_7$ (zirconolite)-$Sm_2Ti_2O_7$ (pyrochlore) System *Journal of European Ceramic Society* 34 2014: pp. 4373 – 4381. https://doi.org/10.1016/j.jeurceramsoc.2014.07.001
14. **Rabanal, M., Várez, A., Amador, U., Dompablo, E., Garcia-Alvarado, F.** Structure and Reaction with Lithium of Tetragonal Pyrochlore-like Compound $Sm_2Ti_2O_7$ *Journal of Materials Processing Technology* 92 – 93 1999: pp. 529 – 533. https://doi.org/10.1016/S0924-0136(99)00211-3
15. **Zhang, Y., Han, C., Zhang, G., Dionysiou, D., Nadagoudaf, M.** PEG-assisted Synthesis of Crystal TiO_2 Nanowires with High Specific Surface Area for Enhanced Photocatalytic Degradation of Atrazine *Chemical Engineering Journal* 268 2015: pp. 170 – 179. https://doi.org/10.1016/j.cej.2015.01.006
16. **Chang, H., Jo, E., Jang, H., Kim, T.** Synthesis of PEG-Modified TiO_2-$InVO_4$ Nanoparticles via Combustion Method and Photocatalytic Degradation of Methylene Blue *Materials Letters* 92 2013: pp. 202 – 205. https://doi.org/10.1016/j.matlet.2012.11.006
17. **Zhang, W., Ma, Z., Du, L., Yang, L., Chen, X., He, H.** Effects of Calcination Temperature on Characterization and Photocatalytic Activity of $La_2Ti_2O_7$ Supported on HZSM-5 Zeolite *Journal of Alloys and Compounds* 695 2017: pp. 3541 – 3546. https://doi.org/10.1016/j.jallcom.2016.11.416
18. **Kubelka, P., Munk, F.** Ein Beitrag zur Optik der Farbanstriche *Technical Physics* 12 1931: pp. 593 – 601.
19. **Zhang, W., Ma, Z., Li, K., Yang, L., Li, H., He, H.** Sol-gel Synthesis of Nano-sized TiO_2 Supported on HZSM-5 *Current Nanoscience* 12 (4) 2016: pp. 514 – 519. https://doi.org/10.2174/1573413712666151223201637
20. **Butler, M.** Photoelectrolysis and Physical Properties of the Semiconducting Electrode WO_2 *Journal of Applied Physics* 48 1977: pp. 1914 – 1920. https://doi.org/10.1063/1.323948
21. **Arthur, H., Nethercot, J.** Prediction of Fermi energies and Photoelectric Thresholds Based on Electronegativity Concepts *Physical Review Letters* 33 1974: pp. 1088 – 1091. https://doi.org/10.1103/PhysRevLett.33.1088
22. **Zhang, G., Zhang, W., Crittenden, J., Chen, Y., Minakata, D., Wang, P.** Photocatalytic Hydrogen Production under Visible-light Irradiation on $(CuAg)_{0.15}In_{0.3}Zn_{1.4}S_2$ Synthesized by Precipitation and Calcination *Chinese Journal of Catalysis* 34 2013: pp. 1926 – 1935. https://doi.org/10.1016/S1872-2067(12)60675-5
23. **Tachikawa, T., Fujitsuka, M., Majima, T.** Mechanistic Insight into the TiO_2 Photocatalytic Reactions: Design of New Photocatalysts *Journal of Physical Chemistry C* 111 2007: pp. 5259 – 5275. https://doi.org/10.1021/jp069005u
24. **Arai, T., Yanagida, M., Konishi, Y., Iwasaki, Y., Sugihara, H., Sayama, K.** Efficient Complete Oxidation of Acetaldehyde into CO_2 over $CuBi_2O_4/WO_3$ Composite Photocatalyst under Visible and UV Light Irradiation *Journal of Physical Chemistry C* 111 2007: pp. 7574 – 7577. https://doi.org/10.1021/jp0725533